Polymer Journal, Vol. 28, No. 3, pp 206—216 (1996)

Normal Modes and Their Dispersion in α Poly(β-benzyl-L-aspartate)

Onkar PRASAD, Poonam TANDON, Vishwambhar Dayal GUPTA,† Shantanu RASTOGI, and Seturam Bandhacharya KATTI*

Physics Department, Lucknow University, Lucknow 226 007, India
**Central Drug Research Institute, Lucknow 226 001, India*

(Received April 3, 1995)

ABSTRACT: Poly(β-benzyl-L-aspartate) (PBLA) is an unusual polypeptide which is capable of going into four different conformations; namely, left-handed α helix, right-handed α helix, ω helix, and β pleated sheet. The present work is a complete study of normal modes and their dispersion in the unusual left-handed α form. A special feature of some dispersion curves is their tendency to bunch in the neighborhood of helix angle. It has been attributed to the presence of strong intramolecular interactions. Crossing and repulsion between the dispersion curves is also observed. The *N*-deuterated analogue of PBLA has been studied to check the validity of assignments and force field (Urey Bradley).†† Specific heat has been obtained from dispersion curves *via.* density-of-states. A comparative study of left-handed and right-handed forms is presented.

KEY WORDS Poly(β-benzyl-L-aspartate) / Conformation / Left-Handed / α Helix / Bunching / Crossover / Repulsion /

In a previous communication in this journal the authors have reported a complete study of normal modes, their dispersion and specific heat as a function of temperature for β poly(L-valine).[1] In continuation of this work, we report similar studies on poly(β-benzyl-L-aspartate) (PBLA) (Figure 1) which is an unusual synthetic homopolypeptide. Under varying conditions of preparation PBLA is capable of adopting four different conformations, namely left-handed α helix, right-handed α helix, ω helix, and β pleated sheet.[2-6] The conformational versatility of PBLA has made it a model of great interest from the view point of molecular dynamics of polypeptides and proteins, specially the reversal of the helix sense which occurs when different ester groups are substituted on polyaspartate backbone *e.g.*, poly(β-methyl-L-aspartate) and PBLA adopt a left-handed conformation with replacement of methyl group by a larger aliphatic one in the former or substitution of a nitro, chloro, cyno group in *para* position of benzyl group in the latter results in reversal of the helix sense.[3] The degree of crystallization and conformational features that undergo change from α to ω and further from ω to β form upon heat treatment, have been successfully correlated with the disposition of side-chains particularly the packing of benzene rings and its effect on the flexibility of side-chain.[2]

X-Ray diffraction, IR absorption, thermal analysis, gas solubility and permeability coefficient studies[4] have led to the conclusion that intramolecularly stacked benzene rings are arranged more regularly in tetragonally packed ω helix (a and $b=13.85$ Å and $c=5.2$ Å) than in hexagonally packed left-handed α form characterized by the meridian reflection at 4.3 Å and a ring at 12.6 Å. The α helix is distorted to some extent at higher temperatures and thus upon heat treatment around 150°C gets readily converted into ω form. The unusual left-handed helix sense both for α and ω helices could be related to the lesser steric hinderances in the left-handed PBLA (α_l PBLA) produced at β carbon atom as compared to the right-handed PBLA (α_r PBLA).[7] Further, the competitive hydrogen bonding between the ester carbonyl group of side-chain and amide group of the backbone precludes the formation of more common right-handed helix.[3] The dihedral angles for the backbone and the side-chain are different in the α_l-PBLA ($\phi=48.6°$, $\psi=58.1°$, $\chi_1=174°$, $\chi_2=20.9°$, $\chi_3=203.4°$, $\chi_4=146.3°$, $\chi_5=24.7°$) and α_r-PBLA. ($\phi=-49.9°$, $\psi=-55.9°$, $\chi_1=305.7°$, $\chi_2=306.3°$, $\chi_3=161.6°$, $\chi_4=228.8°$, $\chi_5=159.6°$).[8] On account of highly favorable non bonded interaction between the side chain and backbone in both the right and left handed α PBLA chain, it has a transverse side chain conformation. This is in-spite-of, unfavorable torsional and electrostatic energy. In this conformation the side chain wraps tangentially about the backbone at right angles to helix axis.[8] The present calculations are based on this conformation.

Polarised infrared studies have shown that the orientation of the side chain ester group differ for right-handed and left-handed α helices. The left-handed form is usually stable in PBLA whereas the right-handed helices are formed in monolayers at the air–water interface. The arrangement of side-chains at the interface probably weakens the interaction between the main chain and the side chain.[6] Quick dried films consist of the left-handed α helical form and slow dried films of the left-handed ω form. However the spectrum of slowly cast films of low molecular weight[6] agrees with that of right-handed α helix. On heat treatment of the left-handed α helix (quick dried) transition is observed to the ω helix. Different conformational change is observed in the slow dried films of low molecular weight (2.3×10^4) heated at 105°C for 15 minutes in vacuum. The film is mostly a mixture of conformations of ω helix, β form, and remanant of α helix. It shows that unstable form of the helix changes to β form by reversion of the helix. On the whole both right- and left-handed α forms have low stabilities and easily transform to ω form.

In continuation of our ongoing work on vibrational analysis and phonon dispersion in a variety of bio-

† To whom all correspondence should be addressed.
†† H. C. Urey and C. A. Bradley, *Phys. Rev.*, **38**, 1969 (1931).

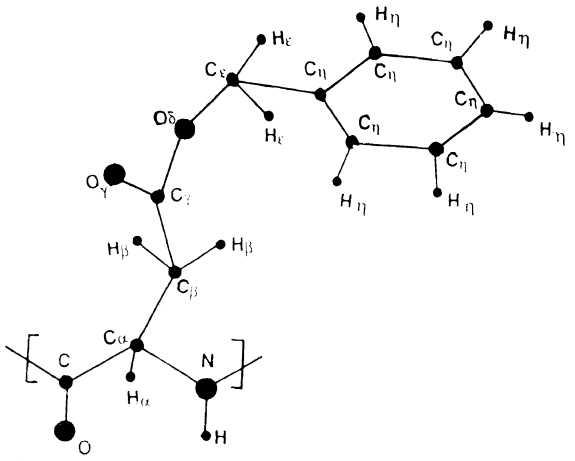

Figure 1. Chemical repeat unit of poly(β-benzyl-L-aspartate).

polymers having α, β, ω, 3_{10} helical, and β sheet conformations,[9-17] we present further studies on vibrational dynamics including heat capacity of α_l PBLA. This left-handed α helical conformation of PBLA is unique because the polypeptides of L-amino acids generally adopt a right-handed α helical conformation. To the best of our knowledge such studies have not been reported for any left-handed α helical polypeptide. Infrared and Raman studies on this have been reported by Frushour *et al.*[5] However, their assignments are both incomplete and are based on qualitative considerations. It is therefore, important to carry out a complete normal mode analysis. The assignments of normal mode frequencies are made on the basis of potential energy distributions (PED) which along with line shape, line intensity, second derivative of the spectra, and presence/absence of the modes in the molecules having atoms placed in similar environment provide better information leading to the assignments of various modes. Further the dispersion curves provide a knowledge of the degree of coupling and the dependence of the frequency of a given mode on the sequence length of ordered conformations. These curves also facilitate correlation of the microscopic behavior of a crystal with its macroscopic properties such as specific heat, enthalpy and free energy.

THEORY AND EXPERIMENT

Calculation of Normal Mode Analysis

The calculation of normal mode frequencies has been carried out according to Wilson's *GF* matrix method[18] as modified by Higgs[19] for an infinite chain. The Wilson *GF* matrix method consists of writing the inverse kinetic energy matrix *G* and the potential energy matrix *F* in internal coordinates *R*. In the case of infinite isolated helical polymer, there are an infinite number of internal coordinates which lead to *G* and *F* matrices of infinite order. Due to the screw symmetry of the polymer a transformation similar to that given by Born and Von Karman can be performed which reduces the infinite problem to finite dimensions. The transformation consists of defining a set of symmetry coordinates

$$S(\delta)=\sum_{s=-\infty}^{+\infty} R^n \exp(is\delta) \tag{1}$$

where δ is the vibrational phase difference between the corresponding modes of the adjacent residue units.

The elements of the $G(\delta)$ and $F(\delta)$ matrices have the form

$$G_{ik}(\delta)=\sum_{s=-\infty}^{+\infty} G_{ik}^{s} \exp(is\delta) \tag{2}$$

$$F_{ik}(\delta)=\sum_{s=-\infty}^{+\infty} F_{ik}^{s} \exp(is\delta) \tag{3}$$

The vibrational secular equation which gives normal mode frequencies and their dispersion as a function of phase angles has the form

$$[G(\delta)F(\delta)-\lambda(\delta)I]=0\,, \quad 0\leq\delta\leq\pi \tag{4}$$

The vibration frequencies $\nu(\delta)$ (in cm^{-1}) are related to eigen values $\lambda(\delta)$ by the following relation

$$\lambda(\delta)=4\pi^2c^2\nu^2(\delta) \tag{5}$$

For any given phase difference δ (other than 0 or π), the $G(\delta)$ and $F(\delta)$ matrices are complex. In order to avoid the difficulties involved in handling complex numbers, methods have been devised to transform the complex matrices into equivalent real matrices by constructing suitable linear combinations of coordinates. One method of transforming a complex matrix to its real matrix equivalent is through a similarity transformation. It can be shown that any complex matrix $H=M+iN$ can be replaced by the real ones

$$\begin{vmatrix} M & -N \\ N & M \end{vmatrix}$$

In the present case, we can write $G(\delta)=G^{R}(\delta)+iG^{I}(\delta)$ and $F(\delta)=F^{R}(\delta)+iF^{I}(\delta)$, where $G^{R}(\delta)$, $F^{R}(\delta)$, $G^{I}(\delta)$, $F^{I}(\delta)$ are the real and imaginary parts of $G(\delta)$ and $F(\delta)$. The product $H(\delta)=G(\delta)F(\delta)$ becomes

$$H(\delta)=\begin{vmatrix} G^{R}(\delta) & -G^{I}(\delta) \\ G^{I}(\delta) & G^{R}(\delta) \end{vmatrix}\times\begin{vmatrix} F^{R}(\delta) & -F^{I}(\delta) \\ F^{I}(\delta) & F^{R}(\delta) \end{vmatrix}$$
$$=\begin{vmatrix} H^{R}(\delta) & -H^{I}(\delta) \\ H^{I}(\delta) & H^{R}(\delta) \end{vmatrix} \tag{6}$$

where

$$H^{R}(\delta)=G^{R}(\delta)F^{R}(\delta)-G^{I}(\delta)F^{I}(\delta) \tag{7}$$

$$H^{I}(\delta)=G^{R}(\delta)F^{I}(\delta)+G^{I}(\delta)F^{R}(\delta) \tag{8}$$

The matrix $H(\delta)$ now has dimensions $2N\times 2N$. The eigenvalues, therefore, occur in pairs of equal values. The difficulty of dealing with complex numbers is thus avoided.

Force Constant Evaluation

The force constants have been obtaied by the least square fitting. In order to obtain the 'best fit' with the observed frequencies the following procedure is adopted. Initially approximate force constants are transferred from α poly(L-alanine)[9] and poly(L-phenylalanine).[14] Thus starting with the approximate *F* matrix F_0 and the observed frequencies λ_{obs} (related through a constant), one can solve the secular matrix equation

$$GF_0L_0=L_0\lambda_0 \tag{9}$$

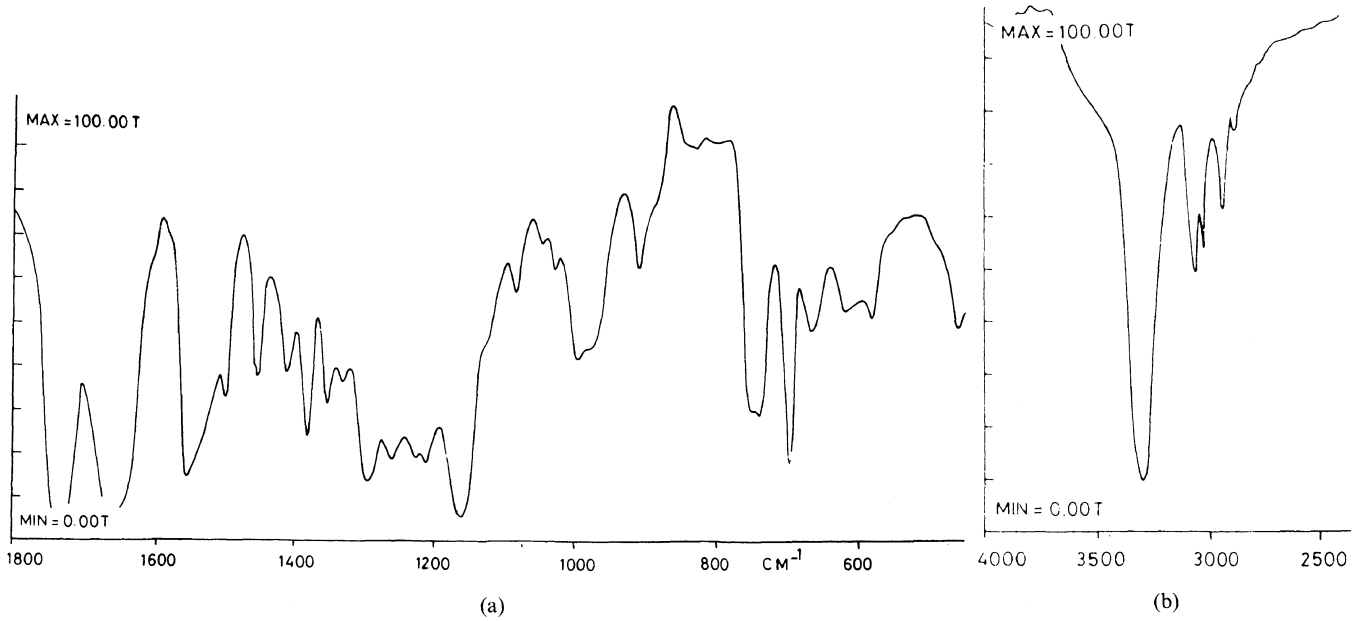

(a) (b)

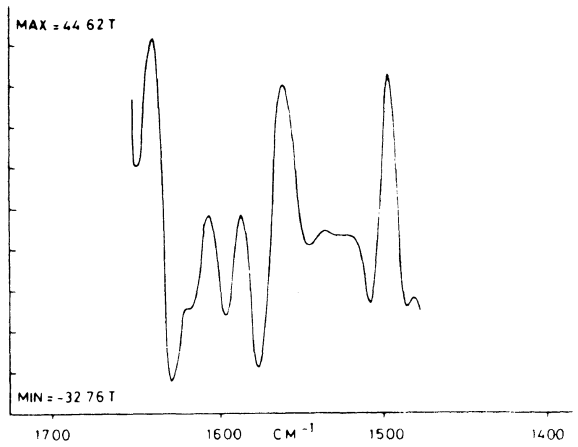

(c)

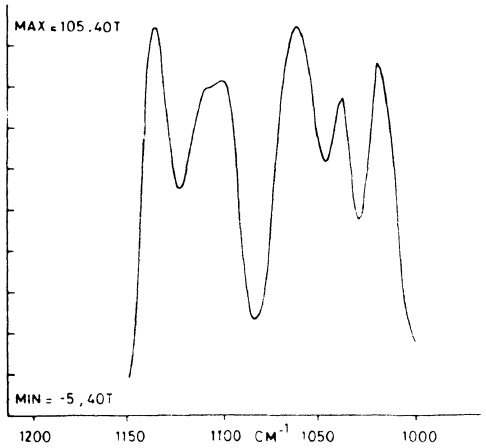

(d)

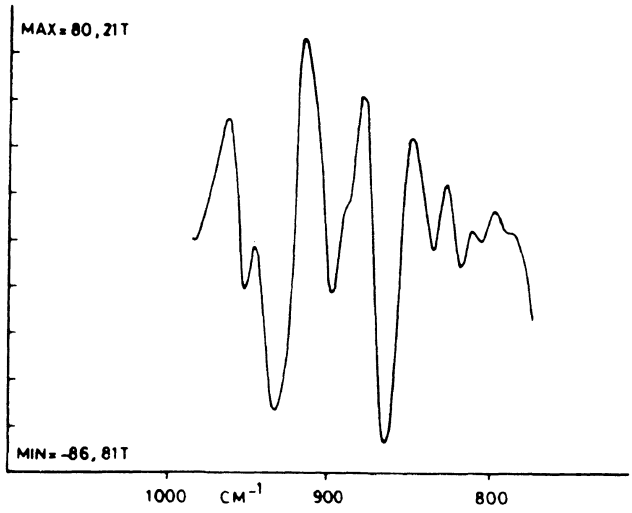

(e)

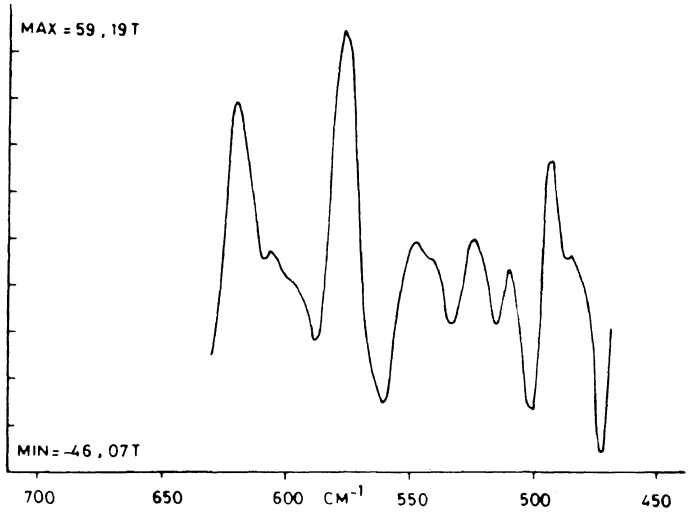

(f)

Let $\Delta\lambda_i = \lambda_{i_{obs}} - \lambda_{i_o}$ in the above equation. It can be shown that in the first order approximation

$$\Delta\lambda = J\Delta F \tag{10}$$

where J is computed from L_o. We wish to compute the corrections to F_o so that the errors $\overline{\Delta\lambda}$ are minimized. We use the theory of least squares and calculate

$$J'P\overline{\Delta\lambda} = (J'PJ)\overline{\Delta F} \tag{11}$$

where P is a weighting matrix and J' is the transpose of

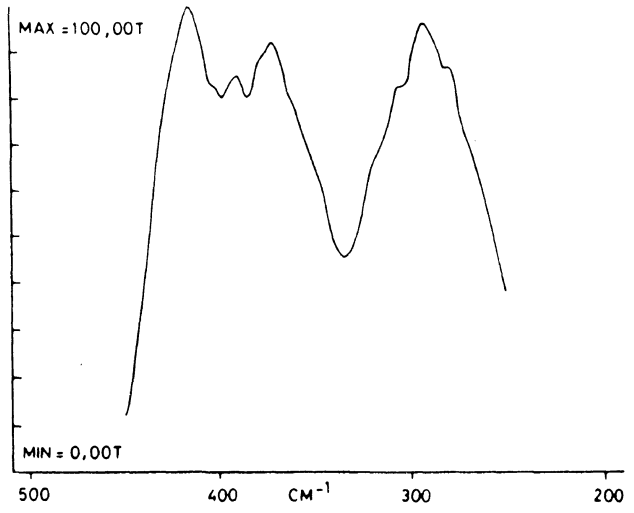

(g)

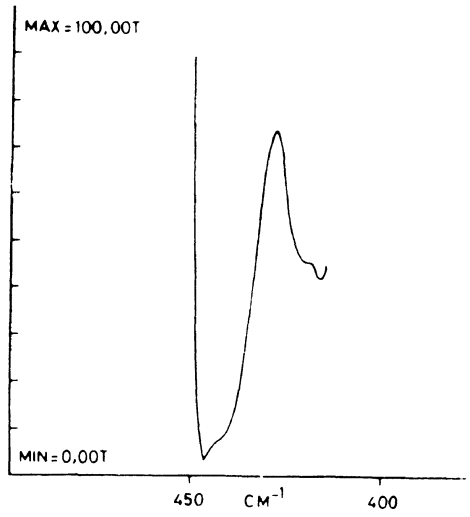

(h)

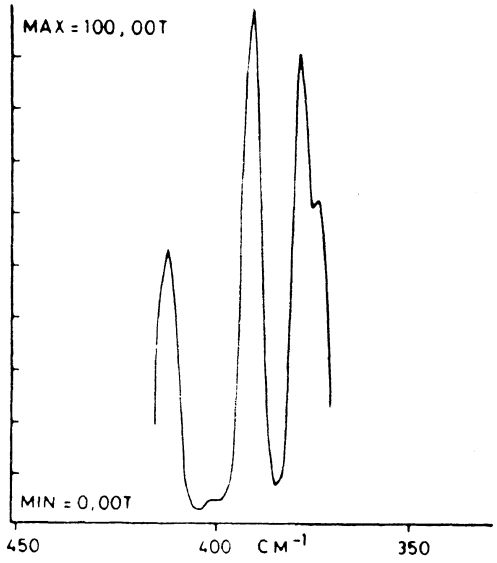

(i)

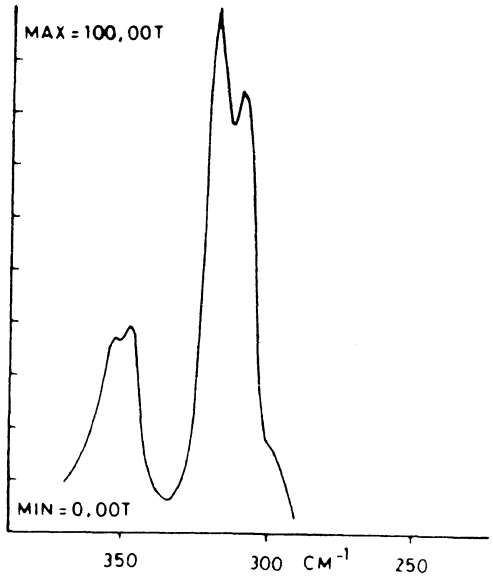

(j)

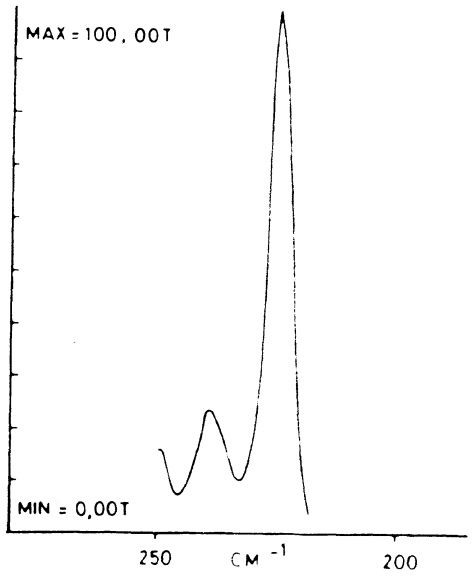

(k)

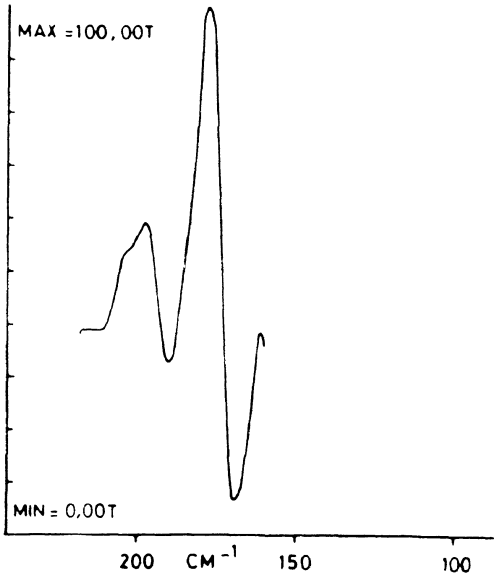

(l)

Figure 2. (a) FT-IR spectra of α_1 PBLA (1800—450 cm^{-1}). (b) FT-IR spectra of α_1 PBLA (4000—2500 cm^{-1}). (c) Second derivative spectra of α_1 PBLA (1675—1475 cm^{-1}). (d) Second derivative spectra of α_1 PBLA (1150—1000 cm^{-1}). (e) Second derivative spectra of α_1 PBLA (1000—775 cm^{-1}). (f) Specond derivative spectra of α_1 PBLA (640—460 cm^{-1}). (g) FT-IR spectra of α_1 PBLA (450—250 cm^{-1}). (h) FT-IR spectra of α_1 PBLA (450—420 cm^{-1}). (i) FT-IR spectra of α_1 PBLA (420—360 cm^{-1}). (j) FT-IR spectra of α_1 PBLA (375—280 cm^{-1}). (k) FT-IR spectra of α_1 PBLA (250—220 cm^{-1}). (l) FT-IR spectra of α_1 PBLA (220—150 cm^{-1}).

J. The solution to this equation is obtained by inverting $(J'PJ)$ to give

$$\overline{\Delta F} = (J'PJ)^{-1} J'P\overline{\Delta\lambda} \tag{12}$$

If the number of frequencies is greater than the number of F matrix elements, the matrix $J'PJ$ should be non singular and we obtain the corrections ΔF which will minimize the sum of the weighted squares of the residuals. If the corrections ΔF are fairly large, the linear relation between force constant and frequency term in the matrix equation 11 breaks down. In such a situation, further refinement using higher order terms in the Taylor's series expansion of $\Delta\lambda_i$ is needed. This procedure has been developed by King and others.[20]

Calculation of Heat Capacity

One of the important uses of dispersion curves is that the microscopic behaviour of a crystal can be correlated with its macroscopic properties such as heat capacity. For a one dimensional system the density-of-state function or the frequency distribution function, which expresses the way energy is distributed among the various branches of the normal modes in the crystal, is calculated from the relation

$$g(\nu) = \sum_j (\partial \nu_j / \partial \delta)^{-1}\big|_{\nu_j(\delta)=\nu} \tag{13}$$

The sum is over all branches j. Considering a solid as an assembly of harmonic oscillators, the frequency distribution $g(\nu)$ is equivalent to a partition function. It can be used to compute thermodynamic quantities such as free energy, entropy, heat capacity and enthalpy.[21] The constant volume heat capacity is obtained using Debye's relation

$$C_v = \sum_j g(\nu_j) k N_A (h\nu_j/kT)^2 \frac{\exp(h\nu_j/kT)}{[\exp(h\nu_j/kT)-1]^2} \tag{14}$$

with

$$\int g(\nu_j)\mathrm{d}\nu_j = 1$$

The constant volume heat capacity C_v, given by eq 14 can be converted into constant pressure heat capacity C_p using the Nernst–Lindemann approximation[22]

$$C_p - C_v = 3RA_o(C_p^2 T/C_v T_m^o) \tag{15}$$

where A_o is a constant often of a universal value $[3.9\times10^{-3}$ (K mol)J$]^{-1}$ and T_m^o is the estimated equilibrium melting temperature, which is taken to be 573 K.[22]

The dihedral angles of backbone as well as side-chain of the α_l PBLA have been taken from the calculations done by Yan *et al.*[8] on the basis of energy minimisation techniques for the various possible conformations of PBLA. The PBLA (Lot# A-28, *MW* 230000) was purchased from Pilot Chemicals, U.S.A. The FT-IR spectra (4000—150 cm^{-1}) was recorded in CsI on Perkin-Elmer 1800 spectrophotometer is shown Figure 2. Before running the spectra the equipment was well purged with dry nitrogen. The spectroscopic data for *N*-deuterated analogue has been taken from Miyazawa *et al.*,[23] respectively.

RESULTS AND DISCUSSION

In α_l PBLA, there are 26 atoms per residue unit, giving rise to 78 dispersion curves. The vibrational frequencies have been calculated for δ values ranging from 0 to π in step of 0.05π. The optically active modes are those for which $\delta = 0, \psi, 2\psi$, where ψ is the angle of rotation about the helix axis which separates the adjacent units. The two lowest lying branches ($\delta = 0$ and $\delta = 5\pi/9$, $\nu = 0$) are four acoustic modes which correspond to the rotation about the helix axis and translations parallel and perpendicular to the helix axis. Since the modes above 1400 cm^{-1} except amides I and II are nondispersive,

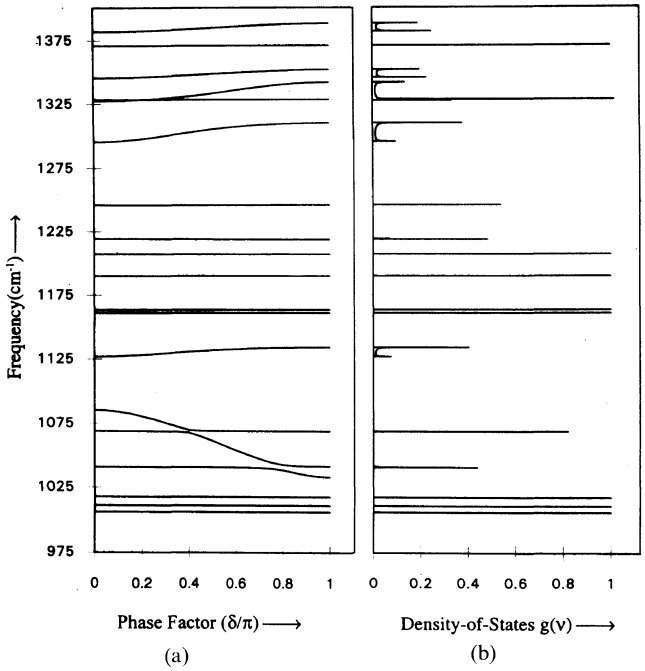

Figure 3. (a) Dispersion curves of poly(β-benzyl-L-aspartate). (1375—975 cm^{-1}). (b) Density-of-states $g(\nu)$ (1375—975 cm^{-1}).

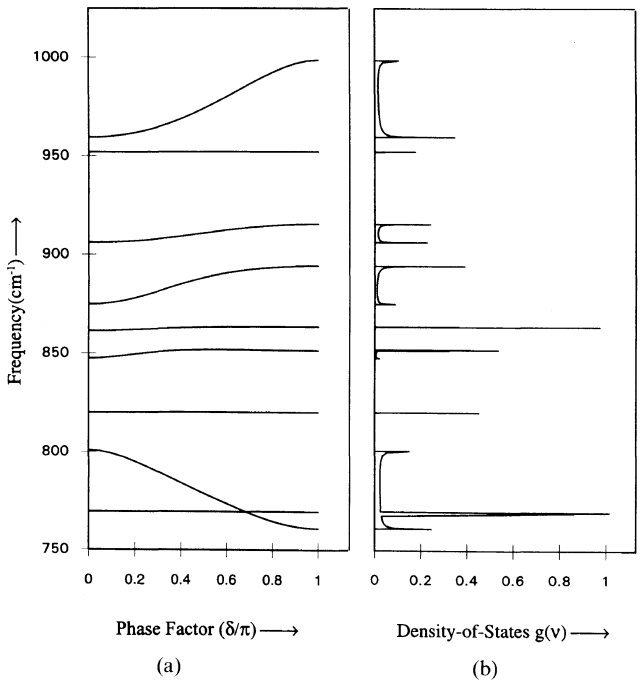

Figure 4. (a) Dispersion curves of poly(β-benzyl-L-aspartate). (1000—750 cm^{-1}). (b) Density-of-states $g(\nu)$ (1000—750 cm^{-1}).

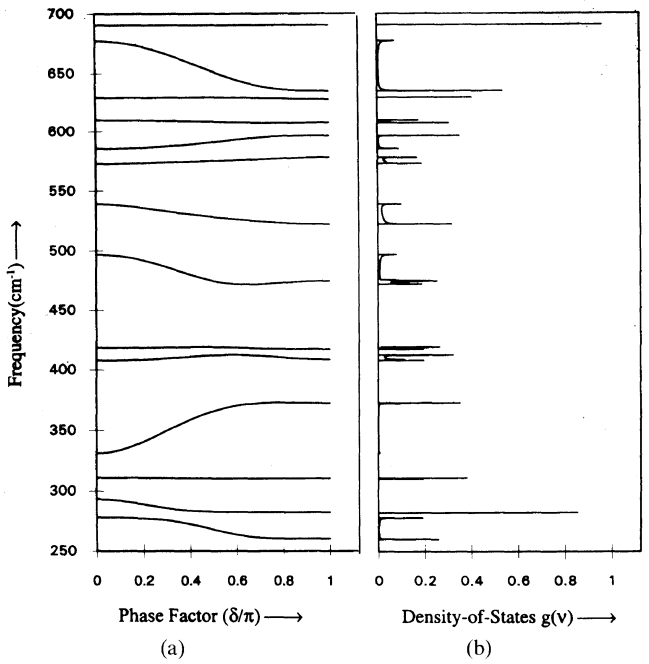

Figure 5. (a) Dispersion curves of poly(β-benzyl-L-aspartate). (700—250 cm^{-1}). (b) Density-of-states $g(\nu)$ (700—250 cm^{-1}).

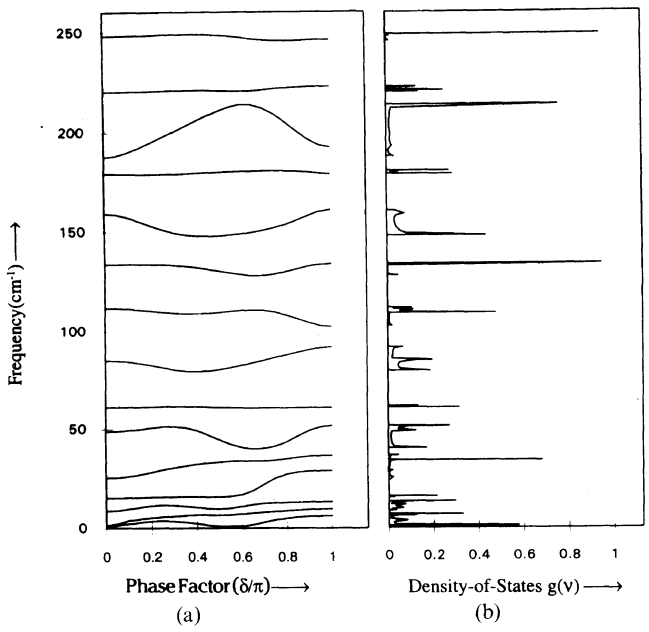

Figure 6. (a) Dispersion curves of poly(β-benzyl-L-aspartate) below 250 cm^{-1}. (b) Density-of-states $g(\nu)$ below 250 cm^{-1}.

only modes below this are shown in Figures 3(a), 4(a), 5(a), and 6(a). Initially the force constants for left-handed α helical backbone have been taken from the right-handed α helical poly(L-alanine)[9] and for side-chain methylene group and benzene ring from poly(L-phenylalanine).[14] They are then modified to give 'best fit' to the spectroscopic data. The final set of force constants are given in Table I. The assignments of the modes, for the sake of simplicity, are discussed under two separate sections *viz.* backbone and side-chain modes.

Backbone Modes

Generally the modes involving the motion of the amide group, N–Cα, Cα–C stretches, C–Cα–N bending are regarded as backbone modes. The normal mode analysis shows that unlike the low frequency region there is very little coupling between skeletal and side chain modes in the 3350—1400 cm^{-1} region. The pure backbone modes are given in Table II at $\delta=0$ and $\delta=5\pi/9$. The backbone modes that mix with side chain modes are given in Table III.

Table I. Internal coordinates and force constants (md $Å^{-1}$)

ν(N=C)	6.300	ϕ(Oδ–Cγ=Oγ)	0.330 (0.80)
ν(N–H)	5.482	ϕ(Cγ–Oδ–Cε)	0.400 (0.45)
ν(N–Cα)	3.300	ϕ(Oδ–Cε–Hεα)	0.390 (0.25)
ν(Cα–Hα)	4.000	ϕ($C\eta_1$–Cε–Hεβ)	0.425 (0.30)
ν(Cα–C)	2.800	ϕ(Hε–Cε–Hε)	0.375 (0.35)
ν(C=O)	8.300	ϕ($C\eta_1$–Cε–Hεα)	0.425 (0.30)
ν(Cα–Cβ)	3.200	ϕ($C\eta_1$–Cε–Oδ)	0.300 (0.45)
ν(Cβ–Cγ)	3.200	ϕ(Cε–$C\eta_1$–$C\eta_2$)	0.720 (0.55)
ν(Cβ–Hβα)	4.200	ϕ(Cε–$C\eta_1$–$C\eta_6$)	0.640 (0.45)
ν(Cβ–Hββ)	4.200	ϕ($C\eta_2$–$C\eta_1$–$C\eta_6$)	0.655 (0.60)
ν(Cγ=Oγ)	10.55	ϕ($C\eta_5$–$C\eta_6$–$C\eta_1$)	0.655 (0.60)
ν(Cγ–Oδ)	4.300	ϕ($C\eta_1$–$C\eta_2$–$C\eta_3$)	0.655 (0.60)
ν(Cε–Oδ)	4.250	ϕ($C\eta_2$–$C\eta_3$–$C\eta_4$)	0.655 (0.60)
ν(Cε–Hεα)	4.250	ϕ($C\eta_3$–$C\eta_4$–$C\eta_5$)	0.655 (0.60)
ν(Cε–Hεβ)	4.250	ϕ($C\eta_4$–$C\eta_5$–$C\eta_6$)	0.655 (0.60)
ν(Cε–$C\eta_1$)	3.500	ϕ($C\eta_1$–$C\eta_2$–$H\eta_2$)	0.370 (0.30)
ν($C\eta_1$–$C\eta_2$)	5.440	ϕ($C\eta_1$–$C\eta_6$–$H\eta_6$)	0.370 (0.30)
ν($C\eta_2$–$C\eta_3$)	5.380	ϕ($C\eta_3$–$C\eta_2$–$H\eta_2$)	0.370 (0.30)
ν($C\eta_3$–$C\eta_4$)	5.440	ϕ($C\eta_2$–$C\eta_3$–$H\eta_3$)	0.370 (0.30)
ν($C\eta_4$–$C\eta_5$)	5.380	ϕ($C\eta_4$–$C\eta_3$–$H\eta_3$)	0.370 (0.30)
ν($C\eta_5$–$C\eta_6$)	5.440	ϕ($C\eta_3$–$C\eta_4$–$H\eta_4$)	0.370 (0.30)
ν($C\eta_6$–$C\eta_1$)	5.380	ϕ($C\eta_5$–$C\eta_4$–$H\eta_4$)	0.370 (0.30)
ν($C\eta_2$–$H\eta_2$)	4.710	ϕ($C\eta_4$–$C\eta_5$–$H\eta_5$)	0.370 (0.30)
ν($C\eta_3$–$H\eta_3$)	4.710	ϕ($C\eta_6$–$C\eta_5$–$H\eta_5$)	0.370 (0.30)
ν($C\eta_4$–$H\eta_4$)	4.710	ϕ($C\eta_5$–$C\eta_6$–$H\eta_6$)	0.370 (0.30)
ν($C\eta_5$–$H\eta_5$)	4.710		
ν($C\eta_6$–$H\eta_6$)	4.710	ω(Cγ–Oγ)	0.410
		ω($C\eta_2$–$H\eta_2$)	0.275
ϕ(C=N–Cα)	0.630 (0.35)	ω($C\eta_3$–$H\eta_3$)	0.275
ϕ(C=N–H)	0.380 (0.59)	ω($C\eta_4$–$H\eta_4$)	0.275
ϕ(Cα–C=O)	0.250 (0.60)	ω($C\eta_5$–$H\eta_5$)	0.275
ϕ(N=C–Cα)	0.210 (0.60)	ω($C\eta_6$–$H\eta_6$)	0.275
ϕ(O=C=N)	0.650 (0.90)	ω(N–H)	0.130
ϕ(Cα–N–H)	0.315 (0.47)	ω(C=O)	0.570
ϕ(N–Cα–Hα)	0.280 (0.80)		
ϕ(N–Cα–C)	0.330 (0.50)	τ(N–Cα)	0.010
ϕ(C–Cα–Hα)	0.425 (0.48)	τ(Cα–C)	0.060
ϕ(Hα–Cα–Cβ)	0.355 (0.48)	τ(Cα–Cβ)	0.030
ϕ(N–Cα–Cβ)	0.220 (0.30)	τ(Cβ–Cγ)	0.025
ϕ(C–Cα–Cβ)	0.450 (0.30)	τ(Cγ–Oδ)	0.032
ϕ(Cα–Cβ–Cγ)	0.480 (0.40)	τ(Cε–Oδ)	0.030
ϕ(Cα–Cβ–Hβα)	0.445 (0.30)	τ(Cε–$C\eta_1$)	0.025
ϕ(Cγ–Cβ–Hβα)	0.445 (0.30)	τ($C\eta_1$–$C\eta_2$)	0.039
ϕ(Hββ–Cβ–Hβα)	0.330 (0.35)	τ($C\eta_2$–$C\eta_3$)	0.035
ϕ(Cα–Cβ–Hββ)	0.445 (0.30)	τ($C\eta_3$–$C\eta_4$)	0.039
ϕ(Cγ–Cβ–Hββ)	0.445 (0.30)	τ($C\eta_4$–$C\eta_5$)	0.035
ϕ(Cβ–Cγ–Oδ)	0.330 (0.50)	τ($C\eta_5$–$C\eta_6$)	0.039
ϕ(Cδ–Cε–Hεβ)	0.390 (0.25)	τ($C\eta_6$–$C\eta_1$)	0.035
ϕ(Cβ–Cγ–Oγ)	0.270 (0.58)	τ(N=C)	0.042

[a] ν, ϕ, ω, τ denote stretch, angle bend, wag, and torsion respectively. Non bonded force constants are given in parentheses.

Amide Modes

The amide groups of polypeptides are strongly chromatophoric in IR absorption and these groups give rise to strong characteristic bands. The correlation between these characteristic bands and conformations have been found to be extremely useful for structural diagnosis of polypeptides and fibrous proteins.[24] A comparison of the amide modes for left-handed and

Table II. Pure Backbone Modes

Calcd	Obsd	Assignments (% PED at $\delta=0$)	Calcd	Obsd	Assignments (% PED at $\delta=5\pi/9$)
3317	3300	ν(N–H) (100) {Amide A}	3317	3300	ν(N–H)(100) {Amide A}
1664	1666	ν(C=O)(57)+ν(N=C)(31) {Amide I}	1661	1666	ν(C=O)(57)×ν(N=C)(31) {Amide I}
1563	1556	ϕ(C=N–H)(32)+ϕ(Cα–N–H)(26)+ν(N=C)(18) {Amide II}	1556	1556	ϕ(C=N–H)(33)+ϕCα–N–H)(27)+ν(N=C)(18) {Amide II}

[a] All frequencies are in cm^{-1}.

Table III. Mixed modes[a]

Calcd	Obsd	Assigments (% PED at $\delta=0$)	Calcd	Obsd	Assignments (% PED at $\delta=5\pi/9$)
2964	2946	ν(Cα–Hα)(73)+ν(Cβ–Hβα)(15)+ν(Cβ–Hββ)(11)	2964	2946	ν(Cα–Hα)(72)+ν(Cβ–Hβα)(16)+ν(Cβ–Hββ)(12)
1382	1386	ϕ(N–Cα–Hα)(29)+ϕ(C–Cα–Hα)(11)+ν(Cγ–Cβ–Hββ)(9)+ν(N–Cα)(9)+ν(Cα–Cβ(7)+ϕ(Cα–Cβ–Hβα)(6)+ν(Cβ–Cγ)(5)+ϕ(Hα–Cα–Cβ)(4)+ϕ(Cγ–Cβ–Hβα)(4)	1385	1386	ϕ(N–Cα–Hα)(29)+ϕ(C–Cα–Hα)(13)+ν(N–Cα)(9)+ν(Cγ–Cβ–Hββ)(9)+ϕ(Cα–Cβ–Hβα)(6)+ν(Cα–Cβ)(5)
1346	1358	ϕ(C–Cα–Hα)(16)+ϕ(N–Cα–Hα)(16)+ϕ(Cγ–Cβ–Hβα)(13)+ν(Cα–Cβ–Hββ)(11)+ν(Cα–Cβ)(10)+ν(Cγ–Cβ–Hββ)(8)+ν(Cβ–Cγ)(7)+ϕ(Cα–Cβ–Hβα)(6)	1349	1358	ϕ(C–Cα–Hα)(16)+ϕ(N–Cα–Hα)(14)+ϕ(Cγ–Cβ–Hβα)(13)+ν(Cα–Cβ–Hββ)(11)+ν(Cα–Cβ)(11)+ν(Cγ–Cβ–Hββ(10)+ν(Cβ–Cγ)(7)+ϕ(Cα–Cβ–Hβα) (7)
1327	1336	ϕ(Hα–Cα–Cβ)(44)+ϕ(C–Cα–Hα)(22)+ν(Cα–C)(7)+ϕ(N–Cα–Hα)(6)	1335	1336	ϕ(Hα–Cα–Cβ)(30)+ν(Cα–C)(17)+ϕ(C–Cα–Hα)(13)+ν(Cα–Cβ)(5)+ϕ(Cα–N–H)(5)+ν(C=O)(5)+ν(N=C)(5)+ϕ(N–Cα–Hα)(4)+ϕ(C=N–H)(4)
1296	1298	ν(N=C)(25)+ν(Cα–C)(14)+ϕ(Cα–N–H)(14)+ν(C=O)(13)+ϕ(C=N–H)(12)+ϕ(O=C=N)(6) {Amide III}	1306	1298	ϕ(Hα–Cα–Cβ)(18)+ν(N=C)(19)+ϕ(C–Cα–Hα)(11)+ν(Cα–C)(9)+ϕ(Cα–N–H)(8)+ϕ(C=N–H)(6) {Amide III}
1127	1113	ν(N–Cα)(56)+ν(Cα–C)(27)	1132	1146	ν(N–Cα)(36)+ν(Cα–Cβ)(25)+ν(Cα–C)(11)+ν(Cα–Cβ–Hββ)(5)
1085	1084	ν(Cα–Cβ)(61)+ν(Cα–Cβ–Hββ)(6)	1057	1046	ν(Cα–Cβ)(29)+ν(N–Cα)(16)+ν(Cα–C)(11)+ν(C=O)(7)+ν(N=C)(7)
959	951	ν(Cγ–Cβ–Hββ)(16)+ϕ(Cα–Cβ–Hβα)(15)+ϕ(Cγ–Cβ–Hβα)(15)+ν(Cα–Cβ–Hββ)(13)	977	996	ν(N–Cα)(12)+ν(Cγ–Cβ–Hββ)(12)+ϕ(Cγ–Cβ–Hβα)(11)+ν(Cα–Cβ–Hββ)(9)+ϕ(Cα–Cβ–Hβα)(7)
875	863	ϕ(O=C=N)(14)+ν(Cα–C)(13)+ϕ(C=N–Cα)(11)+ν(C=O)(9)+ν(Cγ–Oδ)(7)+ω(Cη–Hη)(6)+ν(N=C)(5)	890	898	ϕ(Cα–Cβ–Hβα)(11)+ν(Cα–C)(9)+ν(Cα–Cβ–Hββ)(7)+ϕ(Cγ–Cβ–Hβα)(7)+ω(Cη–Hη)(6)+ϕ(O=C=N)(5)+ν(Cγ–Cβ–Hββ)(5)+ϕ(C=N–Cα)(5)+α(Oδ–Cε–Hεα)(4)
800	806	ω(C=O)(39)+ν(Cα–C)(10)+ϕ(N–Cα–C)(8)	776	—	ω(C=O)(41)+ω(N–H)(16)
677	664	ω(N–H)(40)+ϕ(N–Cα–C)(7)+ω(Cγ–Oδ)(7) {Amide V}	647	664	ω(N–H)(22)+ϕ(O=C=N)(13)+ν(Cα–C)(10)+ω(Cγ–Oδ)(8) {Amide V+IV}
610	616	ω(Cγ–Oδ)(43)+ω(N–H)(11)	608	616	ω(Cγ–Oδ)(38)+ω(N–H)(19)+τ(N=C)(8)+ω(C=O)(5)+τ(Cα–Cβ)(5) {Amide V+VI}
585	589	ϕ(Cη–Cη–Cη)(28)+ϕ(Cγ–Oδ–Cε)(9)+ϕ(Oδ–Cγ–Oγ)(7)	592	580	ϕ(Cη–Cη–Cη)(15)+ω(Cγ–Oδ)(12)+ω(C=O)(11)+ω(N–H)(7)+ϕ(Oδ–Cγ–Oγ)(6)+ϕ(Cγ–Oδ–Cε)(6)
573	561	ω(C=O)(23)+ω(Cγ–Oδ)(10)+τ(N=C)(8)+ω(N–H)(6)+ϕ(Cη–Cη–Cη)(7)+ϕ(Cα–C=O)(5) {Amide VI}	575	580	ϕ(Cη–Cη–Cη)(23)+ω(C=O)(10)+ω(Cγ–Oδ)(9)+ω(N–H)(7)+τ(N=C)(5)+ϕ(Cγ–Oδ–Cε)(5)
497	501	ϕ(Cβ–Cγ–Oγ)(20)+ϕ(Oδ–Cγ–Oγ)(19)+ϕ(N=C–Cα)(10)+ϕ(Cα–C=O)(7)	473	458	ϕ(Cβ–Cγ–Oγ)(22)+ϕ(Cβ–Cγ–Oδ)(7)+ϕ(N=C–Cα)(7)+ϕ(Oδ–Cγ–Oγ)(6)+ϕ(C–Cα–Cβ)(6)+ϕ(Cα–C=O)(6)
332	334	ϕ(O=C=N)(23)+ϕ(Cα–C=O)(19)+ϕ(C=N–Cα)(9)	369	375	ϕ(Cε–Cη–Cη)(20)+ϕ(O=C=N)(8)+ϕ(N–Cα–C)(6)
311	313	ϕ(N–Cα–Cβ)(20)+ϕ(N–Cα–C)(16)+ϕ(Cβ–Cγ–Oγ)(11)	310	313	ϕ(N–Cα–C)(13)+ϕ(Cβ–Cγ–Oγ)(11)+ϕ(Cβ–Cγ–Oδ)(10)+ϕ(Cα–C=O)(6)+τ(Cα–Cβ)(6)
293	302	τ(Cη–Cη)(19)+ϕ(C–Cα–Cβ)(10)+τ(Cε–Cη)(9)	265	268	ϕ(C–Cα–Cβ)(11)+τ(Cη–Cη)(10)+ϕ(N–Cα–Cβ)(6)+τ(Cε–Oδ)(6)+ϕ(Cα–C=O)(6)+ϕ(N–Cα–C)(6)
188	190	ϕ(N=C–Cα)(15)+τ(Cα–Cβ)(12)+τ(Cβ–Cγ)(11)+ϕ(O=C=N)(10)	213	218	ϕ(N=C–Cα)(19)+τ(Cα–C)(16)+τ(Cβ–Cγ)(7)+ϕ(Cα–C=O)(7)
159	169	ϕ(Cγ–Oδ–Cε)(13)+ϕ(Cα–Cβ–Cγ)(13)+τ(Cα–C)(12)	148	—	ϕ(Cγ–Oδ–Cε)(21)+ϕ(Cα–Cβ–Cγ)(14)+τ(Cγ–Oδ)(11)+τ(Cε–Oδ)(9)+τ(Cε–Cη)(5)
134	—	τ(Cγ–Oδ)(17)+τ(Cε–Oδ)(12)+τ(Cε–Cη)(10)+ϕ(Cγ–Oδ–Cε)(8)+ϕ(N–Cα–Cβ)(7)+ϕ(C–Cα–Cβ)(7)	129	—	τ(Cβ–Cγ)(11)+τ(Cα–C)(10)+τ(Cγ–Oδ)(8)+ϕ(C–Cα–Cβ)(6)+τ(Cε–Oδ)(6)+ϕ(C=N–Cα)(6)
112	—	τ(Cα–C)(30)+ϕ(N–Cα–C)(15)+ϕ(C=N–Cα)(9)+τ(Cα–Cβ)(7)+τ(N=C)(7)+τ(N–Cα)(6) {Amide VII}	110	—	τ(Cα–C)(18)+τ(N=C)(8)+τ(Cε–Oδ)(7)+ϕ(Cη–Cε–Oδ)(7)+ϕ(C=N–Cα)(6)+ϕ(Cα–Cβ–Cγ)(6) {Amide VII}
85	—	ϕ(Cη–Cε–Cδ)(20)+ϕ(Cα–Cβ–Cγ)(13)+τ(Cε–Oδ)(12)+ϕ(N–Cα–Cβ)(9)+τ(Cβ–Cγ)(5)+ϕ(Cε–Cη–Cη)(5)	82	—	τ(Cα–C)(14)+τ(Cα–Cβ)(10)+τ(Cβ–Cγ)(7)+ϕ(N–Cα–Cβ)(7)+ϕ(C–Cα–Cβ)(6)
49	—	τ(Cγ–Oδ)(19)+ϕ(C–Cα–Cβ)(18)+τ(Cε–Cη)(15)	42	—	ϕ(Cη–Cε–Oδ)(12)+τ(Cγ–Oδ)(10)+τ(Cε–Oδ)(9)+ϕ(C–Cα–Cβ)(8)+ϕ(N–Cα–Cβ)(7)+τ(Cε–Cη)(7)
26	—	τ(Cη–Cη)(15)+τ(Cα–Cβ)(14)+τ(Cε–Oδ)(8)	34	—	τ(Cγ–Oδ)(11)+τ(Cε–Cη)(8)+τ(Cα–Cβ)(7)+ϕ(N–Cα–Cβ)(6)+ϕ(Cγ–Oδ–Cε)(5)
15	—	τ(Cγ–Oδ)(30)+ϕ(Cα–Cβ–Cγ)(11)+τ(Cη–Cη)(8)	16	—	τ(Cγ–Oδ)(19)+τ(Cη–Cη)(15)+τ(N–Cα–C)(10)+τ(Cα–Cβ)(8)+ϕ(C–Cα–Cβ)(6)+ϕ(N–Cα–C)(6)
9	—	τ(Cα–Cβ)(26)+τ(Cη–Cη)(23)+τ(Cβ–Cγ)(20)	10	—	τ(N–Cα)(13)+τ(Cα–Cβ)(10)+τ(Cη–Cη)(8)+ϕ(N–Cα–Cβ)(8)+ϕ(Cα–Cβ–Cγ)(8)+τ(Cβ–Cγ)(7)+τ(Cγ–Oδ)(7)+ω(N–H)(7)+τ(Cε–Oδ)(6)

[a] All frequencies are in cm^{-1}.

Table IV. A comparision of amide modes in left and right handed α PBLA[a]

	Right-handed α PBLA	Left-handed α PBLA
Amide A	3296	3300
Amide I	1659	1666
Amide II	1553	1556
Amide V	658	664
Amide V + VI	602	616

[a] All frequencies are in cm^{-1}.

Table V. Observed and calculated frequency in *N*-deuterated analogue of α_l PBLA[a]

	Observed	Calculated
Amide A	2440	2421
Amide I	1658	1661
Amide II	1458	1463
Amide V	459	463

[a] All frequencies are in cm^{-1}.

right-handed α helical PBLA is given in Table IV.

In PBLA all the amide modes except amides A and I are dispersive in nature. The amide A band arising due to N–H stretching vibration is itself characteristic of functional group but because of its localised nature it does not reflect the chain conformation. It is sensitive only to the strength of N–H···O=C hydrogen bond. Our N–H stretching frequency calculated at 3317 cm^{-1} is identified well with observed peak at 3300 cm^{-1}. For *N*-deuterated analogue this peak is shifted to 2440 cm^{-1} (Table V) and it is calculated at 2424 cm^{-1}. We have calculated the interatomic distances for both left and right handed α helical PBLA using the dihedral angles given by Yan *et al.*[8] Calculations show that in N–H···O=C the O···H distances are 1.61 Å and 1.66 Å for left and right handed forms respectively (Table VI). It indicates that the hydrogen bond is slightly stronger in case of α_l PBLA as compared with α_r PBLA and not otherwise as reported by Bradbury *et al.*[3] However, since the frequency difference is well within the experimental error, it is difficult to assert either way.

The vibrational modes giving rise to amides I and II bands consist pricipally of the C=O stretch, N–H in-plane bending and C=N stretching modes. These modes are also localised in the amide group and as such are not very sensitive to the conformation of the chain. The amide I calculated at 1664 cm^{-1} is assigned to 1666 cm^{-1}. The frequency difference in amides I, II, and other modes for left and right-handed helices (Table IV) are due to the different arrangement and consequent interaction of β carbon atoms with the backbone. This in turn leads to different dipole–dipole (between the main and side-chains) and non-bonded interactions inducing the frequency shift. The short distances between atoms of the ester group and N–H of the amide groups are given in Table VI. The shorter distances in case of α_l PBLA indicate that there are stronger stabilizing non-bonded interactions between the above mentioned groups in case of left-handed form.

As evidenced from the magnitude and sign of the eigen vectors the amide III mode is the in phase combination

Table VI. A comparison of shortest inter-atomic distances (in Å) between side-chain ester and backbone amide atoms in left and right handed α PBLA

	Right-handed α PBLA	Left-handed α PBLA
$O\delta_1$–H_4	6.50	3.44
$O\delta_1$–N_1	5.26	3.90
$O\gamma_1$–H_4	7.35	3.35
$O\gamma_1$–N_4	8.30	3.83

of N–H in-plane bending and C=N stretching. It is calculated at 1296 cm^{-1} and observed at 1298 cm^{-1}. The contribution of skeletal stretches to the PED of this mode decreases with δ and there is progressive mixing of Hα bending with amide III mode. The mode at 1327 cm^{-1} shows the reverse trend. The Hα bending contribution decreases as one goes away from the zone center.

The amides V and VI consist of asymmetric out-of-plane N–H and C=O vibrations respectively. Owing to large component of N–H out-of plane bending in amide V mode, it is very sensitive to the strength of hydrogen bond.[24] Amide V appears at 677 cm^{-1} ($\delta=0$) and with increase in δ the contributions of ω(N–H) decreases, whereas that of C=O in-plane bending (amide IV) increases. In amide V region, two bands are observed at 664 and 616 cm^{-1} for α_l PBLA, which shift on *N*-deuteration.[23] These bands correspond to the E vibrations calculated at 647 cm^{-1} and 608 cm^{-1}, respectively. The mode calculated at 647 cm^{-1} is largely associated with the N–H out-of plane bending, whereas the other one calculated at 608 cm^{-1} has contributions from both (N–H) and (C=O) out-of-plane bendings. On *N*-deuteration these E vibrations shift to 488 and 463 cm^{-1} (calculated). Although the former mode is not observed, the latter one calculated at 463 cm^{-1} corresponds to the prominent band observed at 459 cm^{-1}.[23]

An interesting feature of the dispersion curve is their tendency to come closer together in groups near the E end. This is indicative of coupling between various modes for the phase value near the helix angle ψ. Similar behavior is also seen in dispersion curves of poly-tetrafluoroethylene (15/7) helix, poly(α-aminoisobutyric acid) 3_{10} helix) and other α helices such as α poly(L-alanine).[9,25,26] For α_l PBLA this feature is prominent for the N–H and C=O wagging modes in the region around 600 cm^{-1} and for skeletal bending modes around 100 cm^{-1}. For modes at 585 and 610 cm^{-1} ($\delta=0$), in the former mode the contributions of ω(C=O) and ω(N–H) keep on increasing steadily and there is dispersion of 11 cm^{-1}. The latter one shows no dispersion. The bending modes in the neighborhood of 100 cm^{-1} involving the angles around the α carbon atom come closer near the helix angle. All the above mentioned modes involve the motion of the nitrogen atom. Thus it seems reasonable to suppose that in all the systems discussed above, the effect can be attributed to the presence of strong intramolecular interactions stabilising the helical structures. The dispersion curves of polyglycine II and other β sheet sample do not show this feature.[10,11] In amide VII band (calculated at 112 cm^{-1}) the PED shows considerable mixing with Cα–N and Cα–C torsions at A as well E ends. As in case of α

poly(L-alanine), in PBLA also there is a certain amount of mixing of the torsional modes with the angle bending modes of the backbone.

Other Skeletal Modes

Apart from amide modes there are several other modes which involve the motion of backbone atoms. The Hα bending mode is calculated at 1327 cm^{-1} ($\delta=0$) and it is identified with observed peak at 1336 cm^{-1}. With increase in δ, the % contribution of skeletal stretch increases and that of Hα bend decreases.

The skeletal stretching mode calculated at 1127 cm^{-1} at zone center corresponds to the observed peak at 1113 cm^{-1}. As δ increases the contributions of ν(N–Cα) and ν(Cα–C) decrease and that of side-chain (Cα–Cβ) stretch increases. The PED of 1085 cm^{-1} mode having (Cα–Cβ) stretch at $\delta=0$ shows just the reverse trend.

The mode appearing at 890 cm^{-1} in the Raman spectra and 898 cm^{-1} in the FT-IR is calculated at 890 cm^{-1}. It mainly comprises of ν(Cα–C), ϕ(O=C=N) and $C\beta H_2$ rock at $\delta=5\pi/9$. At $\delta=0$ the corresponding mode is calculated at 875 cm^{-1} (mixture of skeletal stretch and bending). This mode shows sensitivity to chain conformation because the intensity of this band decreases upon heat treatment due to the conversion of α helical form into β conformation. In the Raman spectra of right-handed α helices, a strong line appears around 930 cm^{-1}, instead of 890 cm^{-1}. This is similar to the case of poly(γ-benzyl-L-glutamate) mode at 931 cm^{-1}, poly(L-leucine) at 931 cm^{-1}, poly(L-glutamic acid) at 931 cm^{-1}, and poly(L-lysine) at 945 cm^{-1}.[27] The skeletal bending mode at 332 cm^{-1} (observed at 334 cm^{-1}) shows maximum dispersion of 42 cm^{-1}. As frequency of the mode increases (with increasing δ values) the contribution of (C=O) in-plane bending to the total PED decreases.

There are a large number of modes which involve the coupling of side chain and backbone motions. Most of these mixed modes show dispersive behaviour, because they are non localised and their motion is coupled to the units further off than the nearest neighbours.

Side-Chain Modes

The side-chain consists of two methylene groups at β and ε positions attached with Cγ=Oγ and Cγ–Oδ–Cε parts of the ester group and terminating with a phenyl ring at η position. Most of the modes due to $C\beta H_2$ group in side-chain are mixed with the vibrations of the back-bone atoms and hence do not appear as pure side chain modes, but benzene ring modes are highly localised and appear as pure modes.

Ring Modes

The vibrational spectrum of α_1 PBLA like poly(γ-benzyl-L-glutamate) (PBLG) is fairly dominated by the vibrations of the benzene ring. Because of being nondispersive, the ring modes along with their assignments are given at $\delta=0$ only. The calculated phenyl ring (Cη–Cη) stretching mode frequencies at 1623, 1599, and 1584 cm^{-1} arise from benzene ring quadrant stretching motions. The observed mode at 1500 cm^{-1} is assigned to the semicircular stretching of the benzene ring and calculated at 1509 cm^{-1}. The ring (Cη–Hη) in-plane bendings are calculated at 1469, 1328, 1190, 1161 cm^{-1} corresponding to reported frequencies at 1456, 1336, 1184, 1166 cm^{-1}, respectively. In the 1456 and 1166 cm^{-1} modes, more than 20% contribution comes from benzene ring ν(Cη–Cη). In 1336 and 1184 cm^{-1} modes, the percentage ring stretching contribution is small.

Table VII. Ring modes[a]

Calcd	Obsd	Assignments (% PED at $\delta=0$)
3051	3066	ν(Cη–Hη)(99)
3046	3034	ν(Cη–Hη)(99)
3045	3034	ν(Cη–Hη)(99)
3043	3034	ν(Cη–Hη)(99)
3042	3034	ν(Cη–Hη)(99)
1623	1627	ν(Cη–Cη)(62)+ϕ(Cη–Cη–Hη)(17)+ϕ(Cη–Cη–Cη)(13)
1599	1596	ν(Cη–Cη)(71)+ϕ(Cη–Cη–Hη)(16)+ϕ(Cη–Cη–Cη)(8)
1584	1576	ν(Cη–Cη)(88)+ϕ(Cη–Cη–Hη)(11)
1509	1500	ϕ(Cη–Cη–Hη)(49)+ν(Cη–Cη)(36)
1469	1456	ϕ(Cη–Cη–Hη)(46)+ν(Cη–Cη)(34)
1328	1336	ϕ(Cη–Cη–Hη)(39)+ϕ(Cη–Cη–Cη)(16)+ν(Cε–Cη)(12)
1190	1184[b]	ϕ(Cη–Cη–Hη)(79)+ν(Cη–Cη)(12)
1161	1166	ϕ(Cη–Cη–Hη)(62)+ν(Cη–Cη)(23)+ϕ(Cη–Cη–Cη)(11)
1069	1084	ν(Cη–Cη)(40)+ϕ(Cη–Cη–Hη)(33)
1018	1028	ϕ(Cη–Cη–Cη)(46)+ν(Cη–Cη)(33)+ϕ(Cη–Cη–Hη)(19)
1011	1028	ν(Cη–Cη)(75)+ϕ(Cη–Cη–Hη)(12)+ϕ(Cη–Cη–Cη)(11)
1006	996	ω(Cη–Hη)(87)+τ(Cη–Cη)(12)
952	951	ω(Cη–Hη)(81)+τ(Cη–Cη)(16)
820	828	ϕ(Cη–Cη–Cη)(29)+ν(Cη–Cη)(29)+ν(Cε–Cη)(24)
770	759[b]	ω(Cη–Hη)(85)+τ(Cη–Cη)(15)
690	698	ω(Cη–Hη)(93)
629	628[b]	ϕ(Cη–Cη–Cη)(72)+ϕ(Cη–Cη–Hη)(15)+ν(Cη–Cη)(9)
418	417	τ(Cη–Cη)(65)+ω(Cη–Hη)(8)
408	404	τ(Cη–Cη)(23)+ϕ(Cε–Cη–Cη)(25)
278	283	τ(Cη–Cη)(60)+ω(Cη–Hη)(12)

[a] All frequencies are in cm^{-1}. [b] Marked frequencies are observed in Roman spectra.

The ring (Cη–Hη) out-of-plane bendings have been calculated at 1006, 952, 861, 770, 690 cm^{-1} corresponding to the observed peaks appearing at 996, 951, 863, 759, 698 cm^{-1}, respectively. The ring in-plane-deformations have been calculated at 1018 and 629 cm^{-1} and they correspond to the observed peaks at 1028 and 628 cm^{-1}, respectively, and ring out-of-plane deformations are assigned to the observed peaks at 417 and 404 cm^{-1} in spectra. These assignments of the ring modes are in order when compared with the corresponding assignments in polystyrene[28] and PBLG.[27]

Other Side-Chain Modes

The pure side chain modes are non dispersive and are shown in Table VIII. The side chain modes which mix with skeletal modes are given in Table III. The band frequency calculated at 1737 cm^{-1} is assigned to well known Cγ=Oγ ester stretching at 1736 cm^{-1} in the observed spectra. This mode appears at 1730 cm^{-1} in case of PBLG.[27] The calculated frequency at 1164 cm^{-1} associated with the Cγ–Oδ–Cε part of the ester, mainly with Oδ–Cε bend adjacent to the carbonyl group is assigned to the observed peak at 1166 cm^{-1} and the corresponding mode appears at 1167 cm^{-1} in the Raman spectra of PBLG.

The scissoring of $C\varepsilon H_2$ methylene group, placed next to the benzene ring, calculated at 1456 cm^{-1} is observed at the same value. Another frequency calculated at 1424 cm^{-1} mainly comprises of scissoring mode of $C\beta H_2$

group adjacent to Cγ=Oγ part of the ester group. All these assignments are consistent with those given by Koenig *et al.*[5,27] for α_1 PBLA and PBLG.

Table VIII. Other pure side-chain modes

Calcd	Obsd	Assignments (% PED at $\delta=0.0$)
2965	2946	ν(Cε–Hεβ)(50)+ν(Cε–Hεα)(49)
2952	2946	ν(Cβ–Hββ)(37)+ν(Cβ–Hβα)(33)+ν(Cα–Hα)(29)
2893	2892	ν(Cε–Hεα)(50)+ν(Cε–Hεβ)(49)
2883	2892	ν(Cβ–Hβα)(50)+ν(Cβ–Hββ)(50)
1737	1736	ν(Cγ=Oγ)(81)+ν(Cγ–Oδ)(7)
1456	1456	φ(Hε–Cε–Hε)(74)
1424	1412	φ(Hβ–Cβ–Hβ)(72)+φ(Cα–Cβ–Hβα)(9) +ν(Cα–Cβ–Hββ)(8)
1371	1386	φ(Cη–Cη–Hη)(33)+ν(Cε–Oδ)(14)+ν(Cε–Cη)(13) +φ(Cη–Cε–Hεα)(10)+ν(Cη–Cε–Hεβ)(9) +φ(Oδ–Cε–Hεα)(8)+ν(Oδ–Cε–Hεβ)(7)
1246	1264	ν(Cγ–Oδ)(35)+ν(Cβ–Cγ)(23)+ν(Cε–Cη)(7)
1219	1230	φ(Cγ–Cβ–Hβα)(19)+ν(Cα–Cβ–Hββ)(18) +ν(Cγ–Cβ–Hββ)(16)+φ(Cα–Cβ–Hβα)(16)
1207	1214	φ(Cη–Cη–Hη)(16)+ν(Cγ–Oδ)(11)+ν(Cβ–Cγ)(11) +ν(Cε–Cη)(9)+φ(Cη–Cη–Cη)(7)+ν(Cη–Cη)(7) +ν(Cγ–Cβ–Hββ)(6)+φ(Cη–Cε–Hεα)(6) +ν(Cδ–Cε–Hεβ)(5)
1164	1166	φ(Cη–Cε–Hεα)(27)+ν(Cη–Cε–Hεβ)(27) +ν(Oδ–Cε–Hεβ)(18)+φ(Oδ–Cε–Hεα)(18)
1041	1046	ν(Cε–Oδ)(54)+ν(Cη–Cη)(9)+ν(Cβ–Cγ)(8)
906	910	φ(Oδ–Cε–Hεα)(17)+ν(Oδ–Cε–Hεβ)(13) +ν(Cη–Cε–Hεβ)(11)+ω(Cη–Hη)(9) +φ(Cη–Cε–Hεα)(9)+ν(Cγ–Oδ)(6)
861	863[b]	ω(Cη–Hη)(65)+τ(Cη–Cη)(12)
848	833	ν(Cγ–Oδ)(22)+ν(Cβ–Cγ)(15)+ν(Oδ–Cε–Hεβ)(7) +ω(Cη–Hη)(6)+φ(Oδ–Cε–Hεα)(4)+φ(Cη–Cε–Hεα)(4)
539	533	φ(Oδ–Cγ–Oγ)(12)+φ(Cβ–Cγ–Oδ)(12) +φ(Cα–Cβ–Cγ)(12)+φ(Cη–Cη–Cη)(8) +φ(Cε–Cη–Cη)(7)+φ(Cη–Cε–Oδ)(7)
248	245	τ(Cε–Oδ)(28)+φ(Cη–Cε–Oδ)(19)+τ(Cη–Cη)(7)
220	218	τ(Cη–Cη)(41)+τ(Cε–Cη)(15)+φ(Cγ–Oδ–Cε)(13)
179	169	τ(Cη–Cη)(37)+τ(Cβ–Cγ)(14)+φ(Cγ–Oδ–Cε)(11)
61	—	τ(Cη–Cη)(36)+τ(Cε–Cη)(21)+τ(Cβ–Cγ)(19)

[a] All frequencies are in cm^{-1}. [b] Marked mode is pure ring mode at $\delta=0$ but as δ progresses ν(Cβ–Cγ) and ν(Cγ–Oδ) start mixing.

The $C\beta H_2$ rocking mode is calculated at 959 cm^{-1} ($\delta=0$) corresponding to the observed peak at 951 cm^{-1} and shows a dispersion of 40 cm^{-1}. The energy of this mode and percentage contribution of ν(N–Cα), ν(Cα–Cβ) increases while that of $C\beta H_2$ rock decreases with increase in δ. The $C\varepsilon H_2$ rock is calculated at 906 cm^{-1} ($\delta=0$) corresponding to the observed peak at 910 cm^{-1}. This mode shows very little dispersion.

Some other characteristic features of the dispersion curves are the repulsion and crossing over of various branches. The two pairs of modes at (1085 and 1069 cm^{-1}) and (1069 and 1041 cm^{-1}) repel each other and exchange character at a particular value of δ. Calculations at very close intervals of $\delta=0.005\pi$ show repulsion and not a crossing over. Such exchange of character and repulsion occur for modes belonging to the same symmetry species. When two approaching modes belong to different symmetry species then alone they can cross.[29] Crossing occurs for (1328.3 and 1327.5 cm^{-1}) and (800 and 770 cm^{-1}) pair of modes. Here one of the modes in the two pairs is non-dispersive. These crossings are observed at different values of δ's. All such modes showing crossover, exchange of character and repulsion are listed in Table IX along with the PED and the δ values at which these features occur.

Specific Heat

The calculated frequency distribution as a function of frequency is shown in Figures 3(b), 4(b), 5(b), and 6(b). Specific heat has been calculated as a function of temperature from dispersion curves *via* density-of-states. The theoretical details have been already given. The predictive values of the specific heat are shown in Figure 7. The contributions of pure back-bone, pure side-chain and mixed modes to the specific heat have also been calculated. The maximum contribution comes from side-chain modes. Heat capacities of β and ω forms of PBLA have also been obtained. They will form the subject

Table IX. Characteristic features of dispersion curves

Freq. ($\delta=0$)	δ^b/π	Before exchange			δ^b/π	After exchange	
		δ^b/π	Freq	PED		Freq	PED
Pair of modes that repel and exchange character							
1085	0.40	0.35	1073	ν(Cα–Cβ)(40)+ν(N–Cα)(11)	0.45	1069	ν(Cη–Cη)(36)+a(Cη–Cη–Hη)(30)
1069	0.40	0.35	1069	ν(Cη–Cη)(38)+ν(Cη–Cη–Hη)(31)	0.45	1065	ν(Cα–Cβ)(34)+ν(N–Cα)(14)
1069	0.70	0.65	1051	ν(Cα–Cβ)(24)+ν(N–Cα)(17)+ν(Cα–C)(11)	0.95	1041	ν(Cε–Oδ)(53)+ν(Cη–Cη)(9)+ν(Cβ–Cγ)(6)
1041	0.70	0.65	1040	ν(Cε–Oδ)(51)+ν(Cη–Cη)(8)+ν(Cβ–Cγ)(7)	0.95	1033	ν(N–Cα)(15)+ν(C=O)(14)+ν(Cα–C)(13) +ν(N=O)(12)
Pair of modes that cross							
Freq. ($\delta=0$)	δ^b/π	Before crossing			δ^b/π	After crossing	
		δ^b/π	Freq	PED		Freq	PED
1328	0.20	0.15	1328	ν(Hα–Cα–Cβ)(40)+ν(C–Cα–Hα)(20)+ν(Cα–C)(8)	0.25	1329	a(Hα–Cα–Cβ)(40)+a(Cα–Cα–Hα)(19)+ν(Cα–C)(9)
1328	0.20	0.15	1328	a(Cη–Cη–Hη)(37)+a(Cη–Cη–Cη)(16) +ν(Cε–Cη)(10)	0.25	1328	a(Cη–Cη–Hη)(37)+a(Cη–Cη–Cη)(16) +ν(Cε–Cη)(11)
801	0.70	0.65	771	ω(C=O)(42)+ω(N–H)(18)	0.75	767	ω(C=O)(46)+ω(N–H)(21)
770	0.70	0.65	770	ω(Cη–H)(82)+τ(Cη–Cη)(15)	0.75	770	ω(Cη–H)(84)+τ(Cη–Cη)(16)

[a] Marked d Corresponds to repulsion/crossing points. [b] Marked d Corresponds to the points before/after repulsion/crossing.

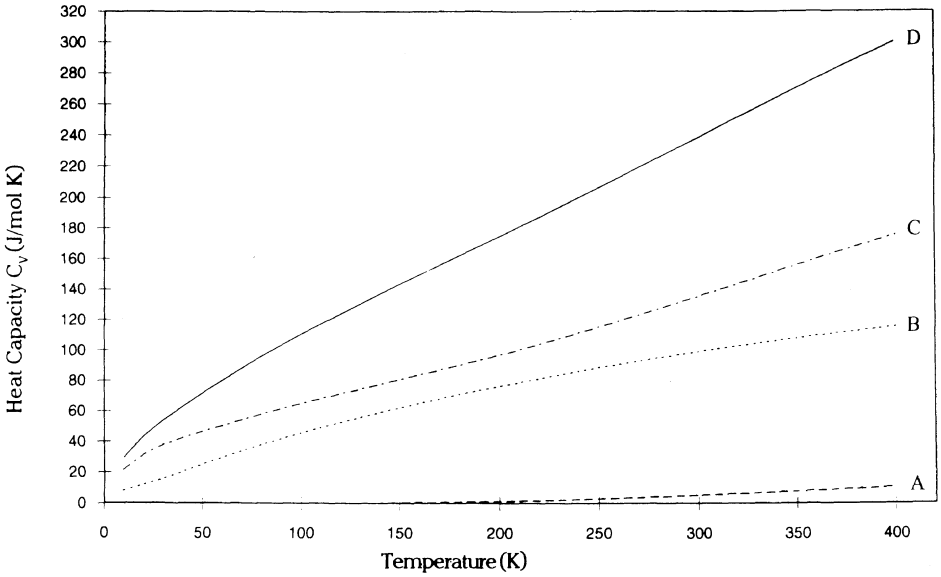

Figure 7. Variation of specific heat C_v with temperature. [The contribution of backbone modes (– – –), mixed modes (------), side-chain modes (–·–·–) and total heat capacity (——) are shown by curves A, B, C, and D, respectively.]

matter of our later publication alongwith phonon dispersion and density-of-states. Briefly, it is observed that the contributions of various modes varies as:

Pure side-chain modes:	$\omega > \alpha_1 > \beta$
Pure backbone modes:	$\omega > \beta > \alpha_1$
Mixed modes	$\beta > \alpha_1 > \omega$

Since specific heat is sensitive to low frequency modes, the above inequalities indicate the weight of such modes in a given conformation.

The contribution from the lattice modes is bound to make an appreciable difference to the specific heat because of its sensitivity to these modes. At the moment, the calculation for dispersion curves for a unit cell are extremely difficult because even if we assume a minimum of two chains in unit cell (as taken in case of ω PBLA[30]) then there would be 208 atoms leading to a matrix of 624×624. It would bring in an enormous number of interactions and make the problem almost intractable. Thus in-spite-of several limitations involved in the calculation of specific heat and absence of experimental data, the present work does provide a good starting point for further basic strudies on thermodynamical behaviour of polypeptides and proteins which go into well-defined conformations.

Acknowledgement. Financial assistance to V.D.G. from the Council for Scientific Research, New Delhi under the Emeritus Scientist Scheme is gratefully acknowledged.

REFERENCES

1. L. Burman, P. Tandon, V. D. Gupta, S. Rastogi, and S. Srivastava, *Polym. J.*, **27**, 481 (1995).
2. H. Obata and H. Kanetsuna, *J. Polym. Sci.*, **9**, 1977 (1971).
3. E. M. Bradbury, B. G. Carpenter, and R. M. Stephens, *Biopolymers*, **6**, 905 (1968).
4. H. Kodama, Y. Tsujita, and A. Takizawa, *J. Macromol. Sci.-Phys.*, **B17(1)**, 57 (1980).
5. B. G. Frushour and J. L. Koenig, *Biopolymers*, **14**, 2115 (1975).
6. H. Kyotani and H. Kanetsuna, *J. Polym. Sci.*, **10**, 1931 (1972).
7. E. M. Bradbury, A. K. Downie, A. Elliott, and W. E. Hanby, *Proc. Roy. Soc. (London), Ser., A*, **259**, 110 (1960).
8. J. F. Yan, G. Vanderkooi, and H. A. Scheraga, *J. Chem. Phys.*, **49**, 2713 (1968).
9. M. V. Krishnan and V. D. Gupta, *Chem. Phys. Lett.*, **6**, 231 (1970).
10. M. V. Krishnan and V. D. Gupta, *Chem. Phys. Letts.*, **7**, 285 (1970).
11. V. D. Gupta, S. Trevino, and H. Boutin, *J. Chem. Phys.*, **48**, 3008 (1968).
12. R. D. Singh and V. D. Gupta, *Spectrochim. Acta*, **27A**, 385 (1971).
13. A. Gupta, P. Tandon, V. D. Gupta, S. Rastogi, and G. P. Gupta, *J. Phys. Soc. Jpn.*, **64**, 315 (1995).
14. L. Burman, P. Tandon, V. D. Gupta, S. Rastogi, S. Srivastava, and G. P. Gupta, *J. Phys. Soc. Jpn.*, **64**, 327 (1995).
15. A. M. Dwivedi and V. D. Gupta, *Chem. Phys. Lett.*, **16**, 909 (1972).
16. V. D. Gupta, R. D. Singh, and A. M. Dwivedi, *Biopolymers*, **12**, 1377, (1973).
17. R. B. Srivastava and V. D. Gupta, *Biopolymers*, **13**, 1965 (1974).
18. E. B. Wilson, J. C. Decuis, and P. C. Cross, "Molecular Vibrations: The Theory of Infrared and Raman Vibrational Spectra, Dover Publications, New YOrk, N.Y., 1980.
19. P. W. Higgs, *Proc. Roy. Soc. (London), Ser. A*, **220**, 472 (1953).
20. W. T. King, I. M. Mills, and B. L. Crawford, *J. Chem. Phys.*, **27**, 455 (1957).
21. T. H. Benzinger, *Nature*, **229**, 100 (1971).
22. R. Pan, M. Verma-Nair, and B. Wunderlich, *J. Therm. Anal.*, **35**, 955 (1989).
23. T. Miyazawa, K. Fukushima, and S. Sugano, in "Conformations of Biopolymers," G. N. Ramchandran, Ed., Academic Press, New York & London, 1967, p 157.
24. S. Krimm and J. Bandekar, *Adv. Protein. Chem.*, **38**, 181 (1986).
25. M. J. Hanon, F. J. Boerio, and J. L. Koenig, *J. Chem. Phys.*, **50**, 2829 (1969).
26. O. Prasad, P. Tandon, V. D. Gupta, and S. Rastogi, *J. Phys. Soc. Jpn.*, **64**, 3100 (1995).
27. J. L. Koenig and P. L. Sutton, *Biopolymers*, **10**, 89 (1971).
28. R. W. Snyder and P. C. Painter, *Polymer*, **22**, 1633 (1981).
29. D. I. Bower and W. F. Maddams, "The Vibrational Spectroscopy of Polymers," Cambridge University Press, Cambridge, 1989, p 154.
30. E. M. Bradbury, L. Brown, A. R. Downie, A. Elliott, R. D. B. Fraser, and W. E. Hanby, *J. Mol. Biol.*, **5**, 230 (1962).